Sensors & Diagnostics

COMMUNICATION

View Article Online
View Journal | View Issue

Cite this: *Sens. Diagn.*, 2024, **3**, 59

Received 20th October 2023,
Accepted 18th November 2023

DOI: 10.1039/d3sd00279a

rsc.li/sensors

Unveiling cellular vitality: peptide fluorescent probes illuminate mitochondrial dynamics and ROS activity†

Ixsoyen Vázquez-Sandoval, Jasmine Bernal-Escalante, Adriana Romo-Pérez and Arturo Jiménez-Sánchez *

This study explored cell-penetrating peptide probes for dynamic cellular vitality tracking. In particular, two mitochondrial-penetrating peptide probes effectively monitored changes in mitochondrial morphology and ROS activity, serving as reliable vitality indicators. Dual-confocal channel monitoring and spectrally-resolved confocal microscopy were employed to trace local structural changes during probe photooxygenation induced by mitochondrial ROS.

Mitochondria are essential organelles for the regulation of cellular bioenergetics and relay the switch to the glycolytic phenotype of malignant cells.[1] They modulate Ca^{2+} ion signaling and reactive oxygen species (ROS) levels.[2] It is widely known that mitochondrial function depends on its physical structure which in turn depends on the cellular function.[3] All these factors are crucial in the cellular health and apoptotic events. In spite of that, the physical/morphological monitoring of organelles in healthy and disease status is uncommon.[4] These changes in mitochondrial morphology, which affect its network organization in response to environmental cues, are known as mitochondrial dynamics.[5] Importantly, prior to directly affecting cell viability (defined as the percentage of live cells in a population), these cellular changes may impair the cell ability to divide without necessarily causing cell death, a phenomenon referred to as cell vitality.[6] Cell vitality is a rather uncommon process used in tissue culture, microbiology and toxicity research, although represents a powerful tool which involves the physiological capabilities of cells.[7] However, while mitochondrial dynamics have been correlated with cell viability,[8] the real-time monitoring of cell vitality during mitochondrial dynamics alterations that not necessarily led to cell death, remains an unmet need. In fact, the release of active caspases and cytochrome *c* before or even in the absence of mitochondrial membrane potential ($\Delta\Psi_m$) depolarization (due to the respiration-driven reestablishment of $\Delta\Psi_m$) represents a source of artifacts when monitoring the initiators of apoptotic events because important morphology alterations and outer membrane rupture can occur before $\Delta\Psi_m$ collapse.[9] For this reason it is crucial to develop fluorescent probes able to track the cell vitality stage. However, no fluorophore chemistry approaches to track dynamic changes in mitochondria to assess cell vitality have been described to date, and the known molecular probes relay on multiple-assay techniques, *i.e.* using rhodamine 123 to determine the mitochondrial membrane potential,[10] fluorescein diacetate to determine enzymes activity,[11] and determination of the cellular ATP content based on the luciferin reaction.[12] This type of approach requires a complex workflow and separate signal recordings that may cause phenotypic drift and analytical bias.

Here we developed a mitochondrial penetrating peptide-based fluorescent probes presenting a mitochondrial membrane potential and photooxygenation processes that allow fluorescence recordings in the TxR (λ_{exc} = 590 nm, λ_{em} = 605 nm) and GFP (λ_{exc} = 480 nm, λ_{em} = 500) channels. This ROS response and the sensibility of the probes to respond to subtle variations of $\Delta\Psi_m$ enable the continuous monitoring of cell vitality. The new mitochondria-penetrating peptide fluorescent probes, termed **De**ad/**Li**ve **C**ell **Cy**aninen**5** (**DeLiCy5**) and **C**oumarin-**343** (**DeLiC-343**), are presented in Fig. 1.

DeLiC probes are dual Dead/Live cell probes with a mitochondrial $\Delta\Psi_m$ dynamic profile enabling a continuous mitochondrial morphology monitoring during apoptotic/necrotic processes as the mitochondrial mass and volume changes are correlated with $\Delta\Psi_m$ variations, a feature that is not affordable with cationic fluorophores since their localization is controlled by the same chemical moieties that serve as reporters.[13] As these fluorescent probes contain mitochondrial penetrating peptide vectors, they do not require a second probe reporter. Thus, common localization

Instituto de Química – Universidad Nacional Autónoma de México, Ciudad Universitaria, Circuito Exterior s/n., Ciudad de México, Coyoacán 04510, Mexico. E-mail: arturo.jimenez@iquimica.unam.mx

† Electronic supplementary information (ESI) available. See DOI: **https://doi.org/10.1039/d3sd00279a**

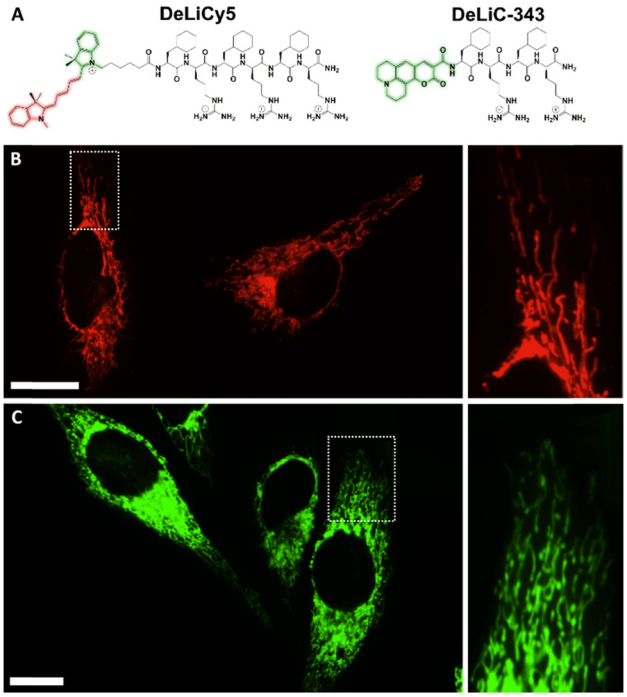

Fig. 1 A) Structure of the mitochondrial fluorescent peptide probes, **DeLiCy5** and **DeLiC-343**. Intracellular localization in live HeLa cells for B) **DeLiCy5** under the Cy5 confocal channel and C) **DeLiC-343** in the GFP channel. The high filamentous-like localization indicates that **DeLiC** probes are mitochondria-specific. Pearson's coefficient = 0.95 and 0.91 for **DeLiCy5** and **DeLiC-343**, respectively (see ESI† for details). Scale bars = 20 μm.

interference and spatial distribution crosstalk problems present in previously reported Dead/Live systems can be overcome.

Notably, a dual-emission channel monitoring was only performed in the case of **DeLiCy5** probe, using the photooxygenation features of Cy5 moiety to detect the presence of singlet oxygen ($^1O_2$) ROS as previously described,[14–16] thus providing an unequivocal cell vitality status tracking.

The **DeLiC** conjugates were obtained by solid-phase synthesis and characterized as described in the ESI file. We found different localization patterns between these probes. **DeLiCy5** is a unique mitochondrial localizer enabling the monitoring of healthy mitochondria in the Cy5 confocal channel with excitation at 647 nm through $\Delta\Psi_m$ dynamic monitoring, while a complementary response for compromised proapoptotic or morphologically altered mitochondria upon subtle ROS stimuli monitored in the green GFP confocal channel when exciting at 488 nm. The analogue **DeLiC-343** on the other hand, exhibited mitochondrial localization only in the GFP channel with $\Delta\Psi_m$ dependence. Colocalizations with MitoLite™ blue localizer are shown in Fig. S7, ESI.† These results highlight the high specificity of the arginine-cyclohexylalanine (Fxr) peptide sequence of the **DeLiC** probes as previously studied.[13,17,18]

To assess the efficiency of the **DeLiCy5** probe undergoing photooxidation, the absorption and emission properties during UV irradiation (300 W Xe lamp) for 25 min translate into a strong deactivation in both, the red-absorption band and the red-fluorescence emission with the simultaneous green-emission increase, highlighting the pi-conjugation breaking, Fig. 2. According to previous literature reports,[13,17–19] and the corresponding mass spectrometry (HRMS) studies, this is assigned to the formation of dioxetane and aldehyde species promoted by singlet oxygen photooxygenation (see Fig. S5, ESI† file), thus activating the green-emission response channel.

We then proceeded to analyze the effect of singlet oxygen photoxygenation *in vitro*, to this end, we utilized 5-aminolevulinic acid (ALA), which is one of the most widely used photosensitizer precursors to produce sufficient singlet oxygen inside the cell in type II photochemical scheme.[20]

The identification of singlet oxygen in the solutions was established by detecting its emission peak at 1270 nm, which had a natural bandwidth of 18 nm.[21] A control experiment was conducted using an air-saturated solution of erythrosin B in anhydrous ethanol, which had an optical density of 0.5. The experiment involved recording single emission peaks at 1270 nm, and this was achieved by employing a 450 W Xe lamp in conjunction with a NIR photomultiplier, (see Fig. S6†). Also, the observed photooxidation and the corresponding selectivity were analysed in terms of *in situ* produced $^1O_2$ by H_2O_2 and HClO reaction in the presence and absence of NaN_3, a selective $^1O_2$ scavenger, the analysis revealed a strong affinity to $^1O_2$ (Fig. S8†). Then, after NaClO and H_2O_2 were added, we recorded 10 minutes before starting light irradiation. Notably, no significant oxidation features were observed in the fluorescence profiles, indicating the probe chemical stability (blue spectra, Fig. S8†).

Thus, photosensitized $^1O_2$ production in HeLa cells influences the spectroscopic features of **DeLiCy5** to activate the green-emission channel around 500 nm with a concomitant red-emission decrease, Fig. 3. This result corresponds to the observed trend in Fig. 2, indicating that both, dioxetane and the aldehyde derivatives (*m*/*z*: 361.2389

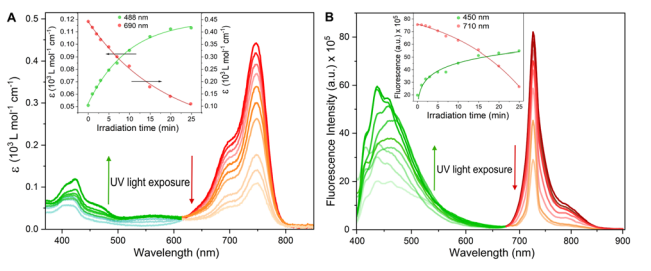

Fig. 2 (A) Ultraviolet–visible (UV–vis) and (B) fluorescence spectra of 16 μM **DeLiCy5** in pH 7.41 HEPES solution upon exposure to 300 W Xe lamp for 25 min to show colour variations. Insets: Calibration profiles using wavelength ranges relevant to the imaging microscopy setup. Arrows show directions of the spectral changes.

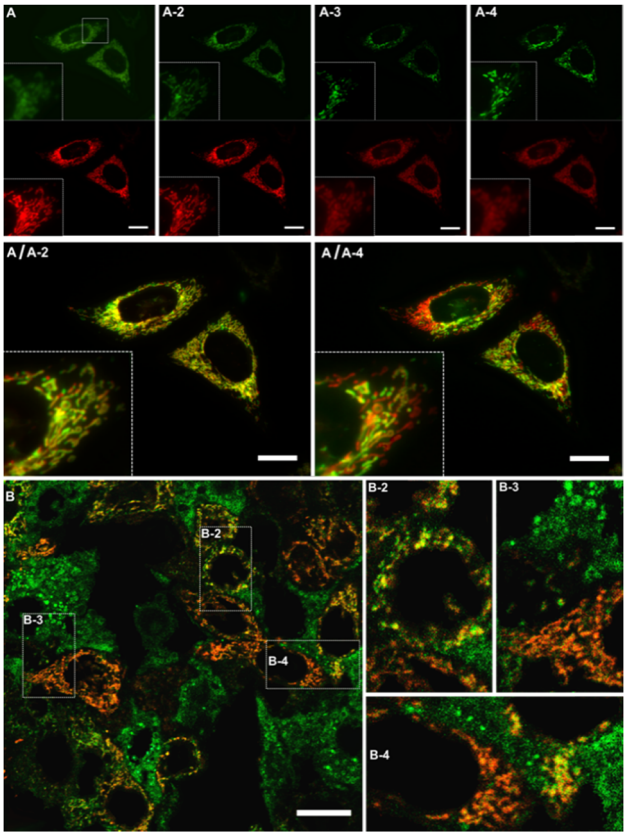

Fig. 3 Time-course monitoring of morphology variations using 5 μM **DeLiCy5** upon ALA-photoinduced $^1O_2$ stimuli in HeLa cells. From panels A to A-4: green and red channels recorded at 5, 10, 15 and 20 min, and overlapped images A(green-channel)/A-2(red-channel) and A(green-channel)/A-4(red-channel). Panels B are green/red overlapped images after 24 hours where live cells still present filamentous-like mitochondria in red and swelled-spherical morphologies predominate in more stressed and apoptotic cells in green. Insets B1 to B4 depict magnified regions. Scale bars represent 20 μm.

and 317.4698, Fig. S5, ESI† file) are formed through the photooxygenation reaction.

The mitochondrial morphology changes induced by ALA-endogenously generated $^1O_2$ were then studied in more detail during time-course experiments, Fig. 3A and B. Specifically, **DeLiCy5** probe enabled to evaluate mitochondrial morphology variations under subtle apoptotic conditions using low-dose ALA photosensitization where interconnected filamentous-like frameworks exhibited red fluorescence (λ_{exc} = 647, λ_{em} = 700 nm) while swelled-spherical morphologies were observed in the GFP green confocal channel, Fig. 3. The robust mitochondrial dynamics indicated a gradual shift from filamentous-like to swollen, rod-shaped, and spherical mitochondria. Some fluorescence stabilization was also noted due to a pronounced signal overlap (depicted in yellow), thus confirming the transitions between these different forms. Notably, as observed in Fig. 3, various cells exhibited a heterogeneous morphology variation when exposed to ALA-induced $^1O_2$ stimuli. However, such cell-to-cell variations gradually became uniform over time.

In fact, 3D (*z*-scan) monitoring after 36 hours indicated a uniform differentiation between live and dead cells in both channels, Fig. S9, ESI† file.

Importantly, the effect of subtle ALA-$^1O_2$ stimuli *vs.* probes mitochondrial localization was analyzed. Interestingly, CCCP depolarization stimuli evidenced clear mitochondrial release for **DeLiC-343**, while for **DeLiCy5** a mitochondrial retention (no dye release) was observed, suggesting that upon photooxidation the Cy5-aldehyde derivative acts as a mitochondrial immobilization group, as previously described,[22] where only mitochondrial permeability transition pore (mPTP) opening resulted in the probe release, Fig. S10.† Additionally, following ALA-induced $^1O_2$ stimuli, 4 hours exposure to 10 μM etoposide, a well-established apoptotic agent for HeLa cells, resulted in the release of the **DeLiCy5** probe from mitochondria, a process not observed when the probe undergoes photodegradation alone, Fig. S11 panel A *vs.* B, ESI† file.

However, to effectively track subtle cellular damage by observing changes in mitochondrial morphology using **DeLiCy5** in live cells over time, it is crucial to mitigate issues related to crosstalk, interference, and signal artifacts. One of the primary challenges in achieving this objective is the loss of structural details and local probe spectral resolution during measurements. In this context, spectrally-resolved confocal microscopy offers distinctive opportunities for analytical bioimaging, providing structural insights of probe responses.

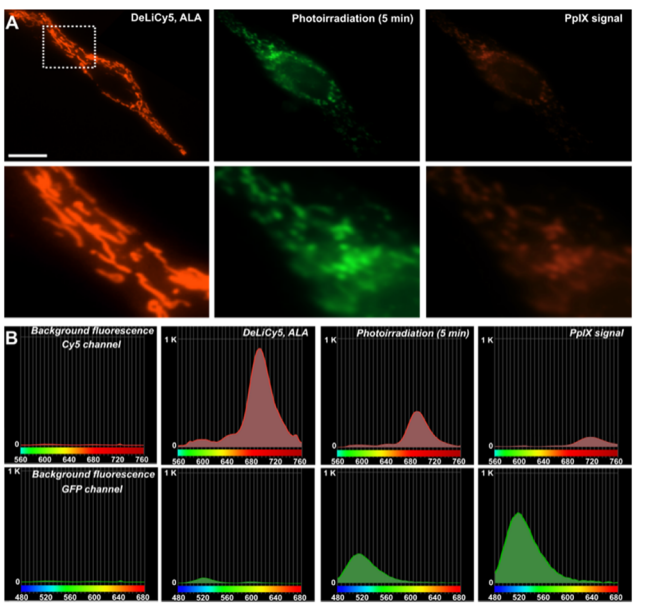

Fig. 4 (A) High-resolution confocal microscopy showing the mitochondrial localization in live HeLa cells of **DeLiCy5** under the Cy5 and GFP channels upon 5 minutes irradiation to visualize first stage vitality decline. The right panels show PpIX signal produced by ALA-photoinduced $^1O_2$ production. Scale bar = 20 μm. (B) Corresponding spectrally resolved confocal microscopy profiles detecting at GFP and Cy5 channels, before and after ALA-photoinduced $^1O_2$ stimuli.

Using a confocal array coupled with a spectral detector unit, accurate spectral unmixing enabled **DeLiCy5** to be spectrally resolved in real time, Fig. 4. As evident from the real-time observations, during apoptosis, there was a steady rise in the diffuse green-fluorescent signal from the outset of the experiment, coupled with a noticeable decline in mitochondrial red fluorescence when employing 488 and 647 nm excitation. This phenomenon consistently aligned with the findings from spectrally-resolved images in Fig. 4B, indicating that the green channel is primarily influenced by the photooxidized Cy5 fluorescence following singlet oxygen photogeneration.

Finally, we investigated the **DeLiCy5** probe imaging capabilities through *in vivo* investigations performed in the zebrafish (*Danio rerio*) model. Then, to demonstrate the **DeLiCy5** ability to sense native $^1O_2$, we examined the injury response in a caudal fin wound, as depicted in Fig. 5. Zebrafish serves as a model system for studying tissue regeneration,[19] aiding in the comprehension of tissue maintenance and turnover processes. The wounded area is predominantly characterized by dead cells. Nonetheless, to investigate subtle, *in vivo* wound healing processes that affect cellular vitality, we employed laser irradiation. Using an erbium:YAG laser (Asclepion) with a frequency of 5 Hz and 7 J cm^{-2} power density, we could swiftly and consistently induce full-thickness wounds on the flank of adult zebrafish.[23] These wounds undergo extremely rapid re-epithelialization, independent of blood clot formation and inflammation.

Through this approach, we successfully tracked the emergence of the initial green-emission signal immediately following erbium:YAG laser tissue injury in real-time and continuously over an extended duration. We then assessed the injury response by employing z-stack time-lapse imaging of the caudal fin, Fig. 5C.

As observed, the region of injured tissue displayed the real-time development of morphologically altered proapoptotic and deceased epithelial cells, marked by a green fluorescence signal. It's recognized that tissue damage leads to the release of various reactive oxygen species (ROS), including superoxide ($O_2^{\bullet-}$) and hydroxyl ($^{\bullet}OH$) radicals, which could potentially trigger lateral reactions of the probe, resulting in fluorescence quenching over extended time periods. However, these outcomes underscore the remarkable sensitivity of **DeLiCy5** in detecting native ROS within the proapoptotic and deceased cells in the wounded tissue.

In conclusion, although **DeLiC-343** probe is also able to localize mitochondria through a $\Delta\Psi_m$ Nernstian interaction, we focused on the **DeLiCy5** fluorescent probe given the Cyanine5 photooxygenation features. **DeLiCy5** has been effectively employed in the exploration of various cell-penetrating peptide probes for the dynamic tracking of cellular vitality. This mitochondrial-penetrating peptide probe reliably monitor alterations in mitochondrial morphology by detecting ROS activity, thus serving as robust vitality indicator. The application of dual-confocal channel monitoring and spectrally-resolved confocal microscopy allowed us to observe and analyze local structural changes during probe photooxygenation, which was triggered by mitochondrial ROS. These findings highlight the utility of **DeLiCy5** in bioimaging applications and provide valuable insights into the assessment of cellular vitality.

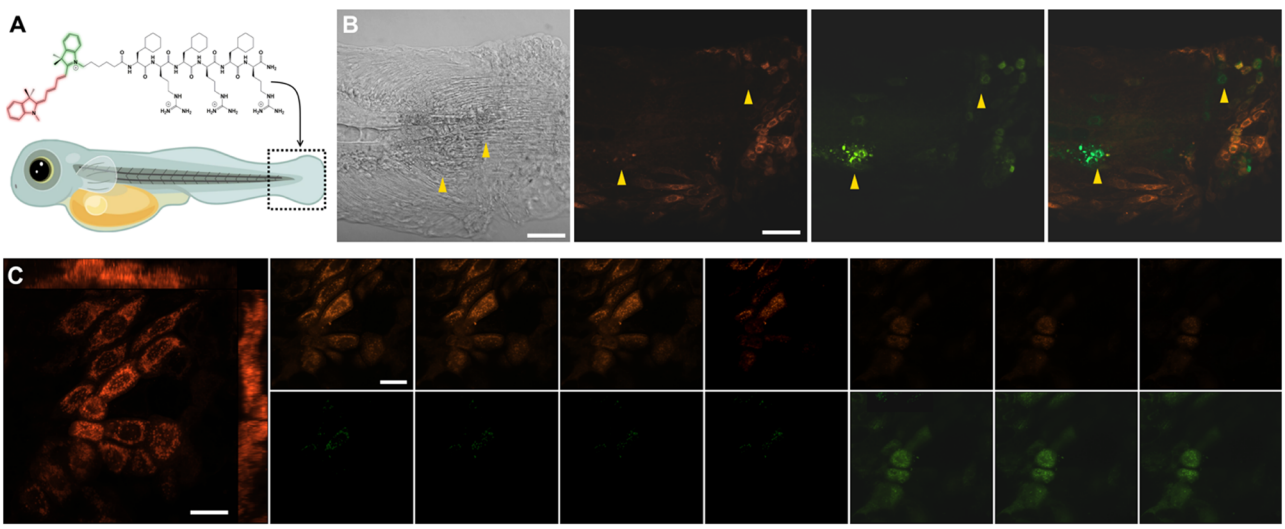

Fig. 5 (A) Confocal imaging of an erbium:YAG laser-induced injury at the caudal fin of zebrafish embryo (48 hpf, hours postfertilization) incubated with 10 μM **DeLiCy5** for 30 min. (B) Bright-field, red-, green-, and overlapped views with yellow triangles delimitating injured zones. (C) *Z*-Scan time-lapse imaging of the caudal fin injured area revealed a dynamic interplay between healthy cells characterized by mitochondrial localization (in red) and the real-time emergence of low-vitality and dead cells. Dead cells were discerned by their lack of mitochondrial localization due to depolarization. Scale bars = 10 μm.

Author contributions

Ixsoyen Vazquez-Sandoval: synthesis and HPLC purification, methodology, analysis; Jasmine Bernal-Escalante: synthesis and chemical characterization, Adriana Romo-Pérez: methodology, tissue culture; Arturo Jiménez-Sánchez: supervision, data analysis, writing – original draft, review & editing.

Conflicts of interest

There are no conflicts to declare.

Notes and references

1 *Mitochondria: The Anti-cancer Target for the Third Millennium*, ed. J. Neuzil, S. Pervaiz and S. Fulda, Springer-Dordrecht, 2014.
2 A. Görlach, K. Bertram, S. Hudecova and O. Krizanova, *Redox Biol.*, 2015, **6**, 260.
3 J. R. Friedman and J. Nunnari, *Nature*, 2014, **505**, 335.
4 D. R. Green and J. C. Reed, *Science*, 1998, **281**, 1309.
5 M. Giacomello, A. Pyakurel, C. Glytsou and L. Scorrano, *Nat. Rev. Mol. Cell Biol.*, 2020, **21**, 204.
6 M. Kwolek-Mirek and R. Zadrag-Tecza, *FEMS Yeast Res.*, 2014, **14**, 1068.
7 E. Colombo, A. De Angelis, C. Bassani, F. Ruffini, L. Ottoboni, L. Garzetti, A. Finardi, G. Martino, R. Furlan and C. Farina, *BMC Neurosci.*, 2023, **24**, 33.
8 L. Simula and S. Campello, *Mitochondrial Bioenergetics*, Springer Protocols, New York, 2018, ch. 15 Monitoring the Mitochondrial Dynamics in Mammalian Cells.
9 F. Ichas, L. S. Jouaville and J.-P. Mazat, *Cell*, 1997, **89**, 1145.
10 E. Marchi and D. Cavalieri, *Genes Nutr.*, 2008, **3**, 159.
11 P. Breeuwer, J. L. Drocourt, N. Bunschoten, M. H. Zwietering, F. M. Rombouts and T. Abee, *Appl. Environ. Microbiol.*, 1995, **61**, 1614.
12 S. Ansehn and L. Nilsson, *Antimicrob. Agents Chemother.*, 1984, **26**, 22.
13 A. Jiménez-Sánchez, E. Lei and S. O. Kelley, *Angew. Chem., Int. Ed.*, 2018, **57**, 8891.
14 Y. Cho, H. J. An, T. Kim, C. Lee and N. K. Lee, *J. Am. Chem. Soc.*, 2021, **143**, 14125.
15 Q. Zheng and L. D. Lavis, *Curr. Opin. Chem. Biol.*, 2017, **39**, 32.
16 J. B. Grimm and L. D. Lavis, *Nat. Methods*, 2022, **19**, 149.
17 S. B. Fonseca, M. P. Pereira and S. O. Kelley, *Adv. Drug Delivery Rev.*, 2009, **61**, 953.
18 S. R. Jean, M. Ahmed, E. K. Lei, S. P. Wisnovsky and S. O. Kelley, *Acc. Chem. Res.*, 2016, **49**, 1983.
19 J. Bernal-Escalante, T. Molina-Villa, F. López-Casillas and A. Jiménez-Sánchez, *ACS Sens.*, 2022, **7**, 2303.
20 J. Chi, Q. Ma, Z. Shen, C. Ma, W. Zhu, S. Han, Y. Liang, J. Cao and Y. Sun, *Nanoscale*, 2020, **12**, 11008.
21 M. Bregnhøj, M. Westberg, B. F. Minaev and P. R. Ogilby, *Acc. Chem. Res.*, 2017, **50**, 1920.
22 S. Zhang, H. Chen, L. Wang, C. Liu, L. Liu, Y. Sun and X. Shen, *J. Mater. Chem. B*, 2021, **9**, 1089.
23 R. Richardson, K. Slanchev, C. Kraus, P. Knyphausen, S. Eming and M. Hammerschmidt, *J. Invest. Dermatol.*, 2013, **133**, 1655.